Analysis and Experimental Verification of a Linear Switched Reluctance Motor Having Special Pole Shape

N.C. Lenin[1], R. Arumugam[2]
1- Department of Electrical Engineering, St. Joseph's College of Engineering, India
Email: nclenin@gmail.com
2- Department of Electrical Engineering, SSN College of Engineering, India
Email: electricalelectronics@rediffmail.com

Received: January 2010 Revised: March 2010 Accepted: May 2010

ABSTRACT:
In this paper, the results of a finite element analysis are carried out on a new stator geometry of a three phase longitudinal flux Linear Switched Reluctance Motor (LSRM). In the new geometry, pole shoes are affixed to the stator poles. Static and dynamic characteristics for the proposed structure have been highlighted. Motor performance for variable load conditions is discussed. The 2-Dimensional (2-D) finite element analysis (FEA) and the experimental results of this paper prove that LSRMs are one of the strong candidates for linear propulsion drives.

KEYWORDS: Linear Switched Reluctance Motor, Finite Element Analysis, Force Ripple

1. INTRODUCTION

Linear switched reluctance motors are attractive alternatives to linear induction or synchronous machines due to lack of windings on the stator or translator structure, easier manufacturing and maintenance, good fault tolerance capability [1]. LSRMs are classified as (a) longitudinal flux (b) transverse flux. This paper is dedicated to the longitudinal flux LSRM. A design procedure for longitudinal-flux LSRM has been described in [2]. Other types of longitudinal-flux LSRMs are presented in [3], with coupled flux paths, and in [4] with uncoupled flux paths for a magnetic levitation system. A high force longitudinal-flux double-sided double-translator LSRM has been analyzed in [5]. Longitudinal-flux LSRMs have been proposed for applications such as precise motion control [6], [7] and as propulsion systems for railway vehicles [8] or vertical elevators [9]–[11]. Recently, a detailed sensitivity analysis of double sided LSRM parameters based on [12] has been presented in [13].

Despite of the various advantages, LSRMs has some drawbacks such as high force ripple, vibration, acoustic noise and need of power electronic converters. Several efforts to reduce or eliminate the torque ripple of the rotary switched reluctance motors (RSRMs) have been presented in the literature [14-18]. Multi phase excitation to reduce the force ripple in the LSRM has been explained in [19]. However, the previous method considerably increases the copper losses. In this paper a novel stator structure for a longitudinal flux LSRM is proposed to reduce the force ripple. Two dimensional (2D) finite element analysis (FEA) is carried out to predict the performance of the conventional and the proposed structures.

A control strategy for the proposed LSRM is dynamically simulated, which consists of force and velocity control loops. A trapezoidal velocity profile is used to control travel position smoothly during acceleration, deceleration, and stop of the motor. Conventional proportional–integral controller is used for the current and velocity control loops [10]. Further, the influence of load variation on some of the parameters like the velocity, current, and the efficiency of the motor are studied.

The organization of the paper is as follows: Section 2 presents new stator geometry for LSRMs that improves the force profile and FEA results for the conventional and the proposed structures. Section 3 contains dynamic simulation results of the proposed structure. Experimental results from the prototype machine and their correlation with FEA results are presented in Section 4. Conclusions and future work are summarized in Section 5.

2. FORCE RIPPLE ANALYSIS USING AN ALTERNATIVE GEOMETRY

2.1. Definition, Sources of the Force Ripple and Techniques to Reduce It

Assuming that the maximum value of the static force as F_{max}, the minimum value that occurs at the

intersection point of two consecutive phases as F_{min}, and the average force as F_{avg}, then the percentage force ripple may be defined as (1)

$$\%\,Force\ Ripple = \frac{F_{max} - F_{min}}{F_{avg}} \times 100 \quad (1)$$

The causes of the force ripple in LSRMs are mainly due to the switching of phase currents into its windings and the highly nonlinear nature of the phase inductance variation when the translator moves. These force pulsations contribute to vibrations and acoustic noise in LSRMs.There are two approaches to force profile improvement. One approach is to suitably shape the input excitation current profile by using an electronic control of the power controllers. The second approach is to modify the geometry of the poles of the stator and translator. This research makes an attempt to examine the force profile by the geometry modifications approach and by providing pole shoes on the stator poles.

2.2. Effect of Stator Pole Shaping on the Force Profile

This sensitivity study aims mainly to determine the improvement in the force profile when the stator pole width gets varied. The conventional LSRM is shown in Figure 1. The specifications of the conventional machine are given in Table 1.

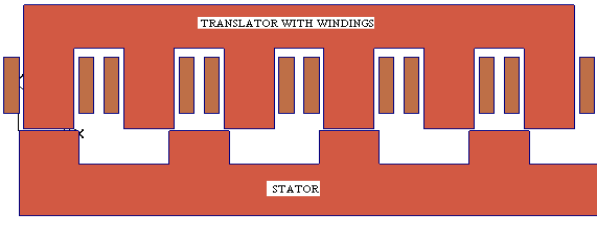

Fig. 1. 2D Cross sectional view of the conventional LSRM

Table 1. Specifications and dimensions of the studied LSRM

l_g = 1.5 mm	w_{sp} = 21 mm
F_{max} = 120 N	h_{sp} = 30 mm
L_{stack} = 40 mm	w_{sy} = 35mm
Steel type (Stator) -M 45	w_{ss} = 31 mm
Steel type (Translator) -M 45	w_{ts} = 26 mm
Travel length= 2 m	h_{tp} = 48 mm
V_{rated} = 120 V	w_{tp} = 13 mm
I_{rated} = 10 A	w_{ty} = 30mm
N_{ph} = 396	Wire size = AWG 18

The width of the stator pole is varied from 16mm to 21mm in steps. The translator geometry remains unchanged throughout the sensitivity study. The height of the stator pole is fixed. The field analysis has been carried out for a phase excitation of 10 A. The predicted propulsion force, normal force, inductances and average force profiles are shown in Figure 2. Table 2 summarizes the comparison of the studied configurations.

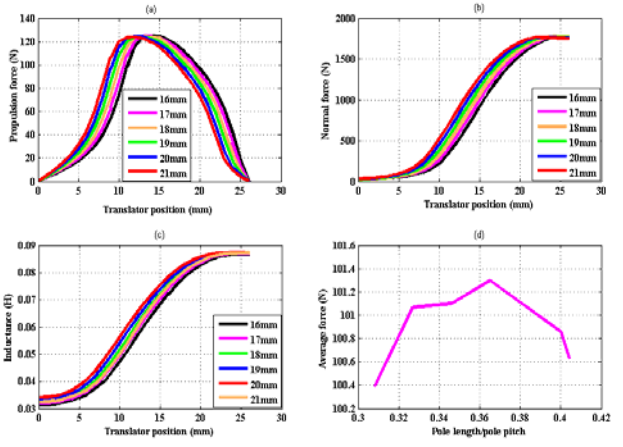

Fig. 2. Force and inductance for various stator pole widths (without pole shoes)

From Table 2 it can be observed that, when the stator pole width is increased, there will be a reduction in the average force, which is not large after a certain point. Figure 2(d) shows the stator pole length/pole pitch vs. average force. From Figure 2(d), we inferred that the maximum average force and low force ripple occurs when the pole width is 19mm.

Table 2. Comparison of force ripple for various stator pole widths (without pole shoes)

W_{sp} (mm)	F_{min} (N)	F_{max} (N)	F_{avg} (N)	% ripple	L_{min} (H)	L_{max} (H)
6	67.33	124.87	100.39	60.38	0.02972	0.08626
17	67.91	124.70	101.07	57.68	0.03019	0.08658
18	68.23	124.57	101.10	55.88	0.03071	0.08683
19	68.32	124.11	101.30	53.41	0.03125	0.087
20	68.28	124.34	100.86	56.16	0.03184	0.08713
21	67.88	123.90	100.63	55.67	0.03246	0.08725

2.3. Force Ripple Minimization Using Stator Pole Shoes

In this section, improving the force profile using stator pole shoes is investigated by 2-D finite-element analysis. The difference between conventional and proposed stator poles are shown in Figure 3. The cross sectional view of proposed LSRM is shown in Figure 4.

The aim in proposing the stator pole shoe is to widen the stator pole width to smoothen the force profile. The analysis is carried out on the conventional LSRM with a pole shoe, which is affixed on the stator poles. The width of the stator pole shoe is 4mm. The stator pole width is varied from 16mm to 20mm in

steps. The width of the pole shoe and overall height of the stator pole are maintained constant. The mutual inductance and leakage effects are neglected. The simulation is presented for an excitation current of 10 A. The predicted propulsion force, normal force and inductance profiles are shown in Fig.5.

(a) **(b)**

Fig. 3. (a) Conventional (b) Proposed Stator poles

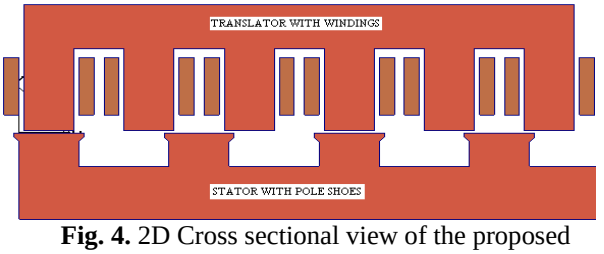

Fig. 4. 2D Cross sectional view of the proposed LSRM

Table 3 summarizes the comparisons of studied configurations with pole shoes. Figure 5(d) shows the stator pole length/pole pitch vs. average force. From Figure 5(d), the maximum average force and low force ripple occurs when the stator pole width is 19 mm with a 4mm pole shoe.

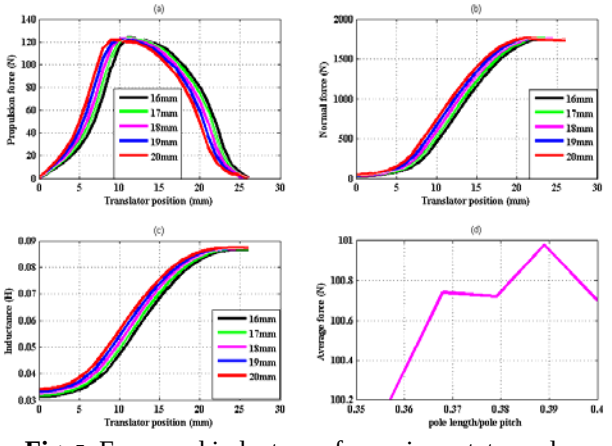

Fig. 5. Force and inductance for various stator pole widths (with pole shoes)

Table 3. Comparison of force ripple for various stator pole widths (with pole shoes)

W_{sp} (mm)	F_{min} (N)	F_{max} (N)	F_{avg} (N)	% ripple	L_{min} (H)	L_{max} (H)
16	69.30	123.33	100.2	53.97	0.03130	0.08681
17	68.83	122.76	100.74	53.54	0.03194	0.08708
18	68.84	122.18	100.72	52.95	0.03260	0.08723
19	68.62	121.78	100.98	52.64	0.03327	0.08730
20	68.27	121.77	100.70	53.12	0.03403	0.08737

2.4. Discussion on 2-D FEA Results

This section addresses an important technical problem in LSRMs, specifically the force ripple. A study of the same by modifying the stator pole affixing stator pole shoes, and the observations made from the 2-D FEA, used for field simulation results on this geometry, are reported. The provision of stator pole shoes improves the force profile and reduces the force ripple at the maximum force regions. Hence, the maximum force is allowed to remain the same for more positions of the translator. The extent of the low force region around the unaligned position is reduced due to the addition of pole shoes. From Table 3 it can be observed that as the stator pole width is increased, keeping the stator pole shoe width as constant, there is a reduction in the average force, which is not large after certain a point. The sensitivity study also depicts that any reduction in the width of the stator pole for the same variations of the pole shoe arcs, contributes to a loss of the average force. It is generally accepted that decreasing the stator pole width will decrease the aligned inductance with negligible effect on the unaligned inductance. This is reflected in Table 2 obtained from a 2-D FEA field simulation. Finally, the stator volume, stator mass and the %force ripple reduction are compared in Table 4. From the Table 4 we inferred that, the proposed LSRM (19 mm stator pole width) has high force density, less force ripple and volume when compared to the conventional machine. So, for other analysis in this paper we prefer LSRM with pole shoe having 19mm pole width.

Table 4. Comparison of volume, mass and force ripple

W_{sp} (mm)	Volume (m^3)		Mass (kg)		Force ripple reduction (%)
	Without pole shoes	With pole shoes	Without pole shoes	With pole shoes	
16	0.00243	0.00238	18.68	18.37	10.62
17	0.00245	0.00242	18.88	18.64	7.18
18	0.00247	0.00245	19.1	18.92	5.24
19	0.0025	0.00249	19.28	19.19	1.44
20	0.00253	0.00252	19.48	19.46	5.41
21	0.00255	NA	19.67	NA	NA

NA: NOT ANALYZED IN THIS PAPER.

3. DYNAMIC SIMULATION

3.1. Force and Velocity Control

For a vertical or horizontal applications, the LSRMs needs a precise control strategy consisting of force, current, velocity, and position controls, as shown in Figure 6. Force control with a force distribution function (FDF) is used to control the LSRM. A trapezoidal velocity profile is used to obtain the desired response curve of the position. In addition, current and

velocity controls with proportional–integral (PI) control for the proposed LSRM are explained in this section. The proposed LSRM is simulated at 0.15 m/s velocity. The data for the dynamic simulation is obtained from the FEA, which is shown in Figure 5. The remaining motor parameters and input specifications are summarized in the Table 1.

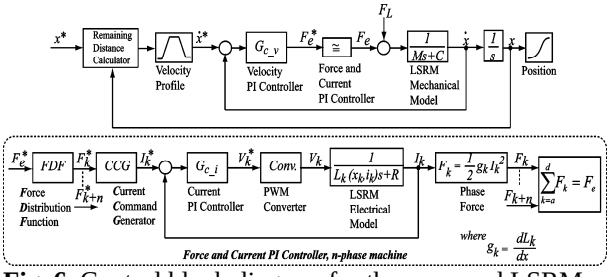

Fig. 6. Control block diagram for the proposed LSRM

During starting, the deceleration command is given at 0.5 m, and during stopping, the deceleration command is given at 0.1 m. The duration for holding at the stop position is set to 1sec. Figure 7 shows the simulation results of the position, velocity, phase current, and generated force of the LSRM at 0.15 m/s.

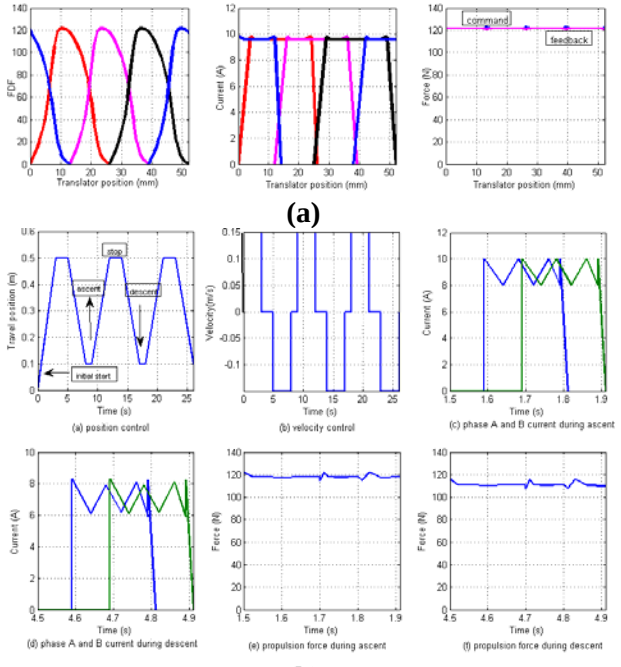

(a)

(b)

Fig. 7. Dynamic analysis (a) Force control (b) Velocity control

In Figure 7 (a) the designed LSRM successfully carries the load at 0.15 m/s producing an excellent velocity and position control performance. After the deceleration command is given at 0.5 m and 0.1 m during starting and stopping respectively, the motor stops at 0.49 m and 0.1 m, where the velocity command from the velocity profile is zero. Under continuous operation, the current amplitude values in starting and stopping are 9.6 and 8.4 A/phase, respectively. In addition, the average force produced is 1191.7 N during acceleration and 113.6 N during deceleration.

3.2. Motor Performance for Variable Load Conditions

In practice, motors operate with changing load conditions. The influence of load variation on some of the parameters like the velocity, current, and the efficiency of the motor are studied. The results shown in Table 5 are obtained when the circuit is turned ON at the point when the inductance starts to increase and turned OFF before it starts to decrease.

Table 5. Influence of load on motor performance

F_L (N)	I (A)	V (m/s)	Input power (W)	Output power (W)	Efficiency (%)
2	2.09	10.42	57.85	26.12	45.15
5	3.28	8.03	65.84	31.46	47.78
10	4.72	6.40	91.39	39	42.67
20	5.31	4.02	114.61	46.99	41
40	6.19	3.35	151.36	57.70	38.12
60	7.87	2.65	181.32	63.66	35.11
80	8.29	1.28	196.36	67	34.12
100	9.79	0.5	214.45	71.11	33.16
120	10.5	0.15	255.84	77.8	30.41

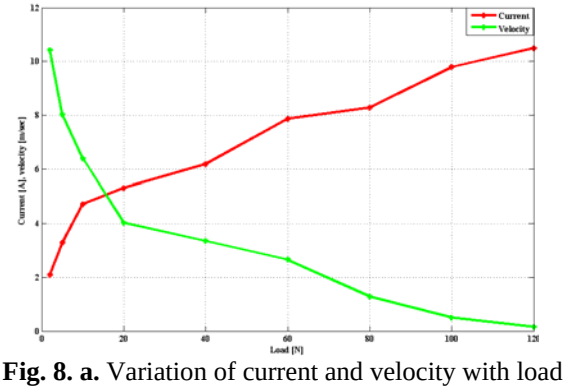

Fig. 8. a. Variation of current and velocity with load

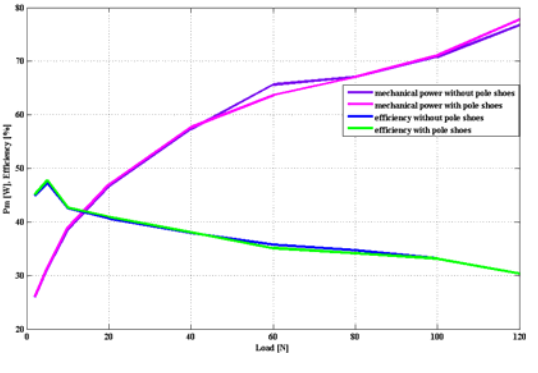

Fig. 8. b. Variation of Pm, efficiency with load

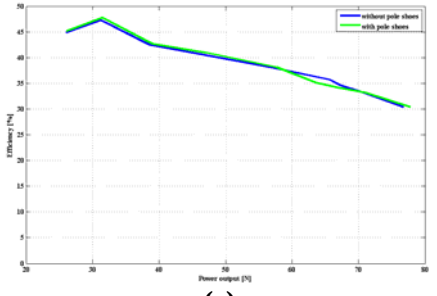

(c)

Fig. 8. c. Variation of efficiency with P_m

Figure 8 (a) shows the velocity and current variation for different load conditions. The velocity steadily decreases with an increase in load. This characteristic reminds of the speed-load characteristic of a series DC motor. Figure 8 (b) shows the characteristics of mechanical power P_m, and the efficiency with change in load. It can be seen that initially as the load increases the efficiency increases and when the load is further increased the efficiency started to decrease. Figure 8 (c) shows the characteristics of the efficiency with change in mechanical power P_m. It can be seen that, the efficiency is high at most of the cases, encouraging the proposal of the pole shoe concept in LSRM.

4. EXPERIMENTAL RESULTS

Figure 9 shows the actual experimental setup for the prototype LSRM with the stator pole shoe that is used as a material carrying vehicle in the laboratory. The experimental road is 2 m long and translator weight is 12 kg. It should be noted that the present setup is intended for development purposes only.

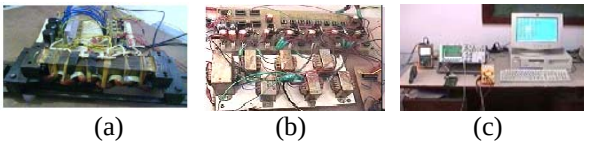

(a) (b) (c)

Fig. 9. Experimental setup of (a) LSRM and converter (b) Driver circuit (c) PC along with measuring instruments

The inductance for the different positions at rated current is measured by locking the translator at each position. A constant current is applied to a phase and is turned off and the falling current profile is computed. The time constant is measured from the profile and hence the inductance is calculated. The measured values of inductance are plotted with the result of FEA results in Figure 10. A comparison of inductance values at aligned and unaligned positions is given in Table 6 at the rated current. Figure 11 shows actual phase voltage and phase current waveforms of the LSRM.

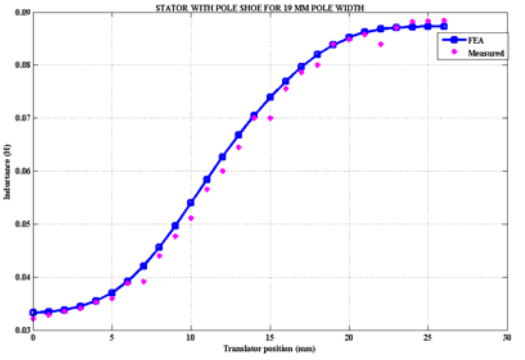

Fig. 10. Comparison of FEA and measured inductance values at rated current

Table 6. Comparison of the calculated and the measured inductance at rated current

Method	Inductance (H)	
	Aligned	Unaligned
FEA	0.0873	0.0332
Measured	0.0884	0.0321

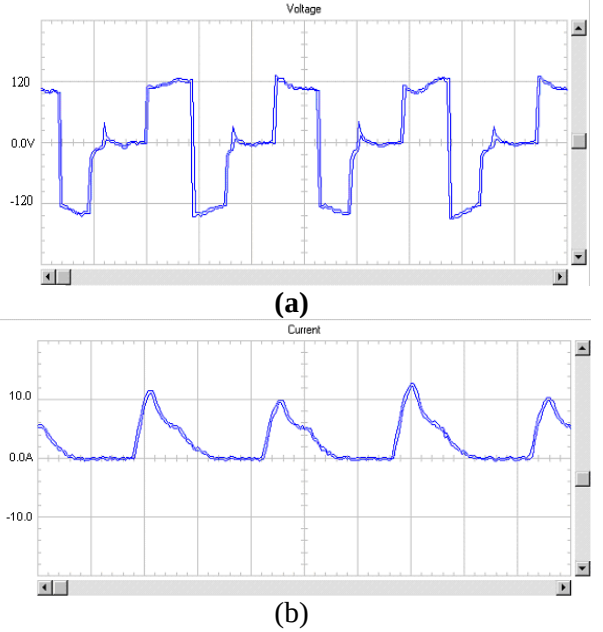

(a)

(b)

Fig. 11. Experimental waveforms during single pulse operation (a) Actual phase voltage of LSRM (b) Actual phase current of LSRM

5. CONCLUSION

A modification of the stator geometry by the provision of stator pole shoes has been presented. A prototype LSRMs is modeled, simulated, analyzed, developed, and experimentally validated with the conventional control strategy. The folowing conclusions are observed when compared to the conventional machine

(a) force ripple is reduced by 5.44%
(b) volume of the stator is reduced by 2.35%
(c) mass of the stator is reduced by 2.44%
(d) Force density is high in the proposed structure
(e) The maximum efficiency occures at a load force of 5N, which is also high when compared to the conventional LSRM.
(f) There is a good agreement between measurement results and FEA values of the inductance profile.

The proposed stator pole shoe geometry research can be further extended to study the thermal, stress and vibration analyses.

6. NOMENCLATURE

w_{sp}	width of the stator pole	(m)
w_{ss}	width of the stator slot	(m)
w_{sy}	stator back iron thickness	(m)
h_{sp}	stator pole height	(m)
w_{tp}	width of the translator pole	(m)
w_{ts}	width of the translator slot	(m)
w_{ty}	translator back iron thickness	(m)
h_{tp}	translator pole height	(m)
l_g	air gap length	(m)
V_{rated}	rated voltage	(V)
I_{rated}	rated current	(A)
V	velocity	(m/s)
F_{max}	maximum force	(N)
F_{min}	minimum force	(N)
F_{avg}	average force	(N)
F_L	load force	(N)
P_m	mechanical power output	(W)
N_{ph}	No. of turns per phase	
L_{stack}	stack length	(m)
L_{min}	minimum inductance	(H)
L_{max}	maximum inductance	(H)
x*	position	(m)
$\dot{x}^*$	commanded velocity	(m/s)
$\dot{x}$	actual velocity	(m/s)
F_e*	commanded force	(N)
F_e	actual force	(N)
k	phase a, b, c.	
f_k	force distribution function	
F_k*	distributed commanded force	(N)
F_{k+n}*	distributed commanded force for N no. phases	(N)
I_k*	current command	(A)
I_k	actual current	(A)
V_k*	reference phase voltage	(V)
V_k	instantaneous phase voltage	(V)
L_k	phase inductance	(H)
x	displacement in propulsion force direction	(m)
g_k	rate of change of inductance with respect to x direction	(N/A^2)

REFERENCES

[1] Miller T.J.E.; Switched Reluctance Motor and Their Control. Hillsboro, OH: Magna Phys., (1993)

[2] Byeong-Seok L., Han-Kyung B., Praveen V. and R. Krishnan; **"Design of a Linear Switched Reluctance Machine",** *IEEE Trans. Ind. Appl*., Vol. 36, No. 6, pp. 1571–1580, (November/December 2000)

[3] Chayopitak N. and Taylor D.G.; **"Design of Linear Variable Reluctance Motor Using Computer-aided Design Assistant",** in Proc. IEEE Int. Conf. Elect. Mach. Drives, pp. 1569–1575, (May 2005)

[4] Sun Z., Cheung N.C., Pan J., Zhao S.W. and Gan W.C.; **"Design and Simulation of a Magnetic Levitated Switched Reluctance Linear Actuator System for High Precision Application",** in Proc. IEEE ISIE, pp. 624–629, (June 30–July 2 2008)

[5] Deshpande U. S., Cathey J. J. and Richter E.; **"High-force Density Linear Switched Reluctance Machine"**, *IEEE Trans. Ind. Appl*., Vol. 31, No. 2, pp. 345–352, (March/April 1995)

[6] Pan J., Cheung N.C. and Yang J.; **"High-precision Position Control of a Novel Planar Switched Reluctance Motor,"** *IEEE Trans. Ind. Electron*., Vol. 52, No. 6, pp. 1644–1652, (December. 2005)

[7] Zhao S.W., Cheung N.C., Gan W.C., Yang J. M. and Pan J. F.; **"A Self-tuning Regulator for the High-precision Position Control of a Linear Switched Reluctance Motor",** *IEEE Trans. Ind. Electron.*, Vol. 54, No. 5, pp. 2425–2434, (October. 2007)

[8] Kolomeitsev L., Kraynov D., Pakhomin F., Rednov F., Kallenbach E., Kireev V., Schneide T.R. and Böcker J.; **"Linear Switched Reluctance Motor as High Efficiency Propulsion System for Railway Vehicles"**, in Proc. SPEEDAM, pp. 155–160, (2008)

[9] Lim H.S. and Krishnan R.; **"Ropeless Elevator with Linear Switched Reluctance Motor Drive Actuation Systems,"** *IEEE Trans. Ind. Electron.*, Vol. 54, No. 4, pp. 2209–2218, (August 2007)

[10] Lim H. S., Krishnan R. and Lobo N. S.; **"Design and Control of a Linear Propulsion System for an Elevator Using Linear Switched Reluctance Motor Drives",** *IEEE Trans. Ind. Electron*., Vol. 55, No. 2, pp. 534–542, (February 2008)

[11] Lobo N. S., Lim H. S. and Krishnan R.; **"Comparison of Linear Switched Reluctance Machines for Vertical Propulsion Application: Analysis, Design, and Experimental Correlation"**, *IEEE Trans. Ind. Appl*., Vol. 44, No. 4,pp. 1134–1142, (July/August 2008)

[12] Arumugam R., Lindsay J.F. and Krishnan R., **"Sensitivity of Pole Arc/Pole Pitch Ratio on Switched Reluctance Motor Performance,"** in Conf. Rec. IEEE IAS Annu. Meeting, Pittsburgh, PA, Vol. 1, pp. 50–54, (October 1988)

[13] Amoros J.G., and Andrada P.; **"Sensitivity Analysis Of Geometrical Parameters on a Double-sided Linear Switched Reluctance Motor,"** *IEEE Transactions on Industrial Electronics*, Vol. 57, No. 1, pp. 311-319, (January 2010)

[14] Schramm D., Williams B.W. and Green T.C., **"Torque Ripple Reduction of Switched Reluctance Motors by Phase Current Optimal Profiling",** Proc. IEEE PESC'92, pp. 857–860, (1992)

[15] Moallem M., Ong C.M. and Unnewehr L.E., **"Effect of Rotor Profiles on The Torque of a Switched Reluctance Motor",** *IEEE Trans. on Ind. Applicat*., Vol. 28, No. 2, pp. 364-369, (March/April 1992)

[16] Hussain I. and Ehsani M.; **"Torque Ripple Minimization in Switched Reluctance Motor Drives by Pwm Current Control"**, *IEEE Trans., on Power Electronics*, Vol. 11, No. 1, pp: 83-88, (January 1996)

[17] Rabinovici R.; **"Torque Ripple, Vibrations, and Acoustic Noise in Switched Reluctance Motors",**, HAIT Journal of Science and Engineering B, Vol. 2, Issues 5-6, pp. 776-786, (July 2005)

[18] Neagoe C., Foggia A. and Krishnan R.; **"Impact of Pole Tapering on the Electromagnetic Force of The Switched Reluctance Motor",** in Conf. Rec. IEEE Electric Machines and Drives Conference, pp. WA1/2.1- WA1/2.3, (1997)

[19] Bae Han-Kyung, Lee B.S., Vijayaraghavan Praveen, Krishnan R.; **"A Linear Switched Reluctance Motor: Converter and Control"**, *IEEE Transactions on Industry Applications*, Vol. 36, No. 5, (September/October 2000)